THE JOURNAL OF PHYSICAL CHEMISTRY A

ARTICLE

pubs.acs.org/JPCA

DFT Study on the Cycloreversion of Thietane Radical Cations

Luis R. Domingo,*[,†] Raúl Pérez-Ruiz,[‡] Juan E. Argüello,[§] and Miguel A. Miranda*[,‡]

[†]Departamento de Química Orgánica, Universidad de Valencia, Dr. Moliner 50, E-46100 Burjassot, Valencia, Spain

[‡]Departamento de Química, Instituto de Tecnología Química UPV-CSIC, Universidad Politécnica de Valencia, Camino de Vera s/n, 46022 Valencia, Spain

[§]INFIQC, Departamento de Química Orgánica, Facultad de Ciencias Químicas, Universidad Nacional de Córdoba, Ciudad Universitaria, 5000 Córdoba, Argentina

Supporting Information

ABSTRACT: The molecular mechanism of the cycloreversion (CR) of thietane radical cations has been analyzed in detail at the UB3LYP/6-31G* level of theory. Results have shown that the process takes place via a stepwise mechanism leading to alkenes and thiobenzophenone; alternatively, formal [4 + 2] cycloadducts are obtained. Thus, the CR of radical cations **1a,b**$^{\bullet+}$ is initiated by C2−C3 bond breaking, giving common intermediates **INa,b**. At this stage, two reaction pathways are feasible involving ion molecule complexes **IMCa,b** (i) or radical cations **4a,b**$^{\bullet+}$ (ii). Calculations support that **1a**$^{\bullet+}$ follows reaction pathway ii (leading to the formal [4 + 2] cycloadducts **5a**). By contrast, **1b**$^{\bullet+}$ follows pathway i, leading to *trans*-stilbene radical cation (**2b**$^{\bullet+}$) and thiobenzophenone.

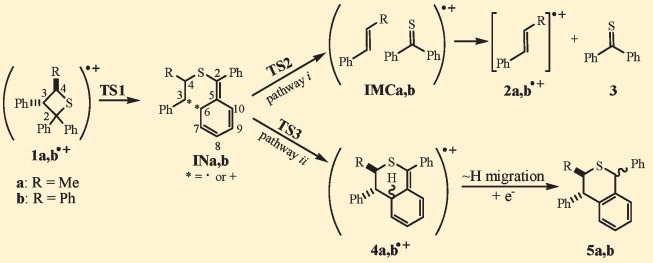

INTRODUCTION

Photoinduced electron transfer (PET) processes have attracted considerable interest over the last decades; they have emerged as fundamental tools in mechanistic and synthetic organic photochemistry and appear to be involved in key biological processes.[1] It is known that PET cycloreversion (CR) of oxetanes and azetidines is potentially involved in the photoenzymatic repair of the (6−4) photoproducts of DNA dipyrimidine sites by photolyases.[2] During the last years, this type of reaction has been extensively studied by our research group, in order to gain insight into mechanistic aspects.[3] Theoretically, the molecular mechanism of the CR of oxetane radical cations has been studied at the UB3LYP/6-31G* level. The process follows a concerted but asynchronous mechanism, where C−C bond breaking at the transition state is more advanced than O−C breaking, allowing a favorable rearrangement of the oxetane radical cations to the alkene radical cations.[4]

By contrast, few examples can be found in the literature related to PET CR of thietanes that mimics the analogous reaction of oxetanes. Thus, reductive cleavage of a thymine-derived thietane leads to photoproducts arising from CR of the four-membered ring.[5] Likewise, ring splitting of 2,2-diarylthietane derivatives under oxidative PET conditions has been achieved using 9,10-dicyanoanthracene (DCA) as sensitizer.[6] Based on fluorescence quenching measurements, generation of sulfide radical cations (not detected) by electron transfer to the DCA singlet excited state has been proposed.

More recently, we have presented an experimental study on the oxidative PET CR of model thietanes, where the involvement of radical cations has been supported by means of laser flash photolysis (LFP).[7] Combination of photoproduct studies and transient absorption measurements has provided convincing evidence for the role of ion−molecule complexes (IMCs) in the mechanism. In addition, the outcome of the reaction has been found to be structure-dependent. Thus, thietane **1a** gives rise to formation of 2-thia-1,2,3,4-tetrahydronaphthalene derivative **5a**, whereas the expected CR products **2b** and **3** are obtained in the case of the tetraphenyl analogue **1b** (Scheme 1).

With this background, it appeared interesting to undertake a detailed theoretical analysis of the splitting mode of thietane radical cations, in order to ascertain whether the CR mechanism takes place along stepwise or concerted processes and to explain the influence of substituents on the preferred reaction pathways. For this purpose, calculations based on DFT methods at the UB3LYP/6-31G* level of theory have been performed, using **1a**, **b** as model compounds.

COMPUTATIONAL METHODS

Theoretical DFT calculations were carried out using the B3LYP[8] exchange-correlation functional, together with the standard 6-31G* basis set.[9] This methodology has been recently used in the study of the photodimerization of cyclohexadiene.[10] The spin-unrestricted (UB3LYP) formalism was used for the open-shell (doublet) radical cations. The S^2 expectations for the doublet states of radical cations

Received: January 7, 2011
Revised: March 30, 2011
Published: May 11, 2011

Scheme 1

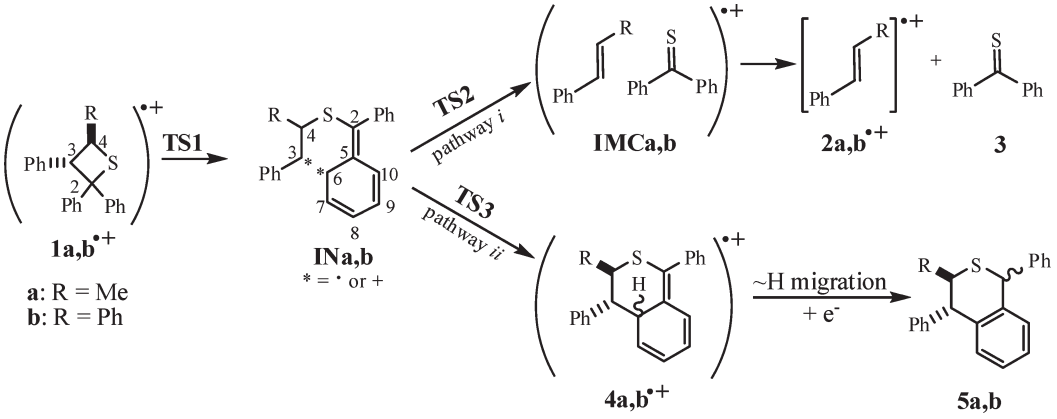

all showed an ideal value (0.750) after spin annihilation, so the geometries and energetics are reliable for this study. Optimizations were carried out using the Berny analytical gradient optimization method.[11] Frequency calculations were performed on all structures to confirm that reactants, intermediates, and products do not have imaginary frequencies and that transition state (TS) structures have only one imaginary frequency. The intrinsic reaction coordinate (IRC)[12] path was traced in order to check the energy profiles connecting each TS with the two associated minima of the proposed mechanism by using the second-order González–Schlegel integration method.[13] The electronic structures of stationary points were analyzed by the natural bond orbital (NBO) method.[14] Solvent effects of acetonitrile (ε = 35.69) were considered at the same level of theory by single point energy calculations of the gas-phase structures using a self-consistent reaction field (SCRF)[15] based on the polarizable continuum model (PCM) of the Tomasi's group.[16] Values of enthalpies, entropies, and free energies in acetonitrile were obtained by frequency calculations over the UB3LYP/6-31G* gas-phase geometries. Thermodynamic calculations were made with the standard statistical thermodynamics at 298.15 K and 1 atm, and harmonic vibrational frequencies were scaled by a factor of 0.96.[17] All calculations were carried out with the Gaussian 98 suite of programs.[18]

RESULTS AND DISCUSSION

The PET CR of thietanes **1** to yield alkenes **2** and thiobenzophenone (TBP) **3**, or formal [4 + 2] cycloadducts **5**, was found to take place along a stepwise mechanism, sharing common intermediates (see Scheme 1). These reactions are initiated by generation of radical cations **1a,b**$^{\bullet+}$. Subsequent C2–C3 bond breaking leads to formation of intermediates **INa,b**, which undergo reaction pathways i and ii. The former results in CR, giving **2** and **3** via an ion–molecule complex IMC, whereas the latter gives rise to formal [4 + 2] cycloadducts **5**, via radical cations **4**$^{\bullet+}$, respectively.

Reaction Pathways of Thietane Radical Cations. Analysis of the potential energy surface (PES) for the CR of **1a**$^{\bullet+}$ to yield the radical cation of *trans*-β-methylstyrene (**2a**$^{\bullet+}$) and TBP **3** indicates that it proceeds through a stepwise mechanism. In principle, cleavage of the thietane ring can be initiated by C2–C3 or S–C4 bond breaking. In acetonitrile, the activation energies associated with these processes are 0.9 (**TS1a**) and 23.8 (**TS1a′**) kcal/mol (see Table 1). In view of the high energy barrier associated with initial S–C4 splitting, this pathway can be safely ruled out. The very low activation energy found for C2–C3 bond breaking in the radical cation **1a**$^{\bullet+}$ points to irreversible conversion of this species into intermediate **INa**, which is actually located 15.9 kcal/mol below **1a**$^{\bullet+}$. Similar results were obtained for **1b**$^{\bullet+}$, which is converted via **TS1b** (2.1 kcal/mol) into intermediate **INb**, located 15.5 kcal/mol below **1b**$^{\bullet+}$.

At this stage, two competitive reaction pathways are feasible. Thus, S–C4 bond breaking would result in formation of **2a,b**$^{\bullet+}$ and **3** after escaping from the corresponding ion–molecule complexes **IMCa,b** (pathway i). On the other hand, intramolecular attack of C3 onto C6 would lead to the formal [4 + 2] cycloadduct **4a,b**$^{\bullet+}$ (pathway ii).

The activation barriers for S–C4 bond breaking in intermediates **INa,b** are also very low: 2.9 kcal/mol at **TS2a** and nearly negligible at **TS2b**. However, while **IMCa** is located 2.5 kcal/mol above **INa**, **IMCb** is located 5.8 kcal/mol below **INb**. Note that for the CR of **1a**$^{\bullet+}$ the separated fragments **2a**$^{\bullet+}$ and TBP **3** are located 7.6 kcal/mol above **INa** (see Table 1).

Table 1. UB3LYP/6-31G* Total Energies (in au) and Relative Energies (in kcal/mol, in Parentheses, Relative to the Corresponding Thietane Radical Cation), in Gas Phase and in Acetonitrile, for the Stationary Points Involved in the CR of 1a,b$^{\bullet+}$

species	gas phase	acetonitrile
1a$^{\bullet+}$	−1248.288215	−1248.353700
TS1a	−1248.288112 (+0.1)	−1248.352201 (+0.9)
TS1a′	−1248.246440 (+26.2)	−1248.315694 (+23.8)
INa	−1248.316315 (−17.6)	−1248.379008 (−15.9)
TS2a	−1248.311833 (−14.8)	−1248.374443 (−13)
IMCa	−1248.311674 (−14.7)	−1248.375052 (−13.4)
2a$^{\bullet+}$ + **3**	−1248.279255 (+5.6)	−1248.366857 (−8.3)
TS3a	−1248.298269 (−6.3)	−1248.364738 (−6.9)
4a$^{\bullet+}$	−1248.314685 (−16.6)	−1248.382810 (−18.3)
1b$^{\bullet+}$	−1440.026794	−1440.092142
TS1b	−1440.023691 (+1.9)	−1440.08874 (+2.1)
INb	−1440.052801 (−16.3)	−1440.116836 (−15.5)
TS2b	−1440.052703 (−16.3)	−1440.116745 (−15.5)
IMCb	−1440.060571 (−21.2)	−1440.126152 (−21.3)
2b$^{\bullet+}$ + **3**	−1440.042171 (−9.6)	−1440.125737 (−21.1)
TS3b	−1440.033712 (−4.3)	−1440.10187 (−6.1)
4b$^{\bullet+}$	−1440.050539 (−14.9)	−1440.120154 (−17.6)

dx.doi.org/10.1021/jp200177a |J. Phys. Chem. A 2011, 115, 5443–5448

The activation barriers associated with intramolecular attack of the C3 carbon atom of intermediates **INa,b** to C6 present similar values: 9.0 (**TS3a**) and 9.4 (**TS3b**) kcal/mol. Formation of the [4 + 2] cycloadduct radical cation is exothermic by −2.4 ($\mathbf{4a}^{\bullet+}$) or −2.1 ($\mathbf{4b}^{\bullet+}$) kcal/mol. Therefore, the nature of the C4 substituent (methyl or phenyl) does not produce any remarkable change along reaction pathway ii.

Analysis of the energy profiles for the two competitive pathways (Figure 1) indicates that a major difference between the PET CR of thietanes **1a,b** is the relative stability of **IMCa,b** compared to **INa,b**. While formation of **IMCa** is endothermic, formation of **IMCb** (ultimately leading to *trans*-stilbene radical cation $\mathbf{2b}^{\bullet+}$ and TBP **3**) is exothermic.

Thermodynamic Analysis. Thermodynamic calculations were performed for all stationary points involved in the reactions of $\mathbf{1a,b}^{\bullet+}$. The total and relative free energies computed at 25 °C in acetonitrile are given in Table 2.

A comparison of the relative energies in acetonitrile given in Table 1 with the relative free energies given in Table 2 shows that the trends are essentially coincident. Only dissociation of **IMCa, b** into CR products $\mathbf{2a,b}^{\bullet+}$ + **3** presents a significant energy difference as a result of the entropy increase associated with this process (56.4 and 54.1 cal/(mol K), respectively). In this context, the negative ΔG values obtained for the free ions by means of B3LYP/6-31G* must be overestimated as indicated by thermodynamic calculations performed using the MPWB1K[19] hybrid meta DFT method, which yield correctly a much less exergonic process for dissociation of **IMCa** than for **IMCb** (see Table S1 in the Supporting Information).

Formation of intermediates **INa** and **INb** is strongly exergonic by −18.3 and −17.5 kcal/mol, respectively. Consequently, C2−C3 bond breaking via **TS1a** (0.3 kcal/mol) and **TS1b** (1.7 kcal/mol) can be considered irreversible. From these intermediates, formation of **IMCa** and **IMCb** takes place with a low activation free energy: 4.4 kcal/mol for **TS2a** and nearly negligible for **TS2b**. However, while the process for **IMCa** is endergonic by 4.1 kcal/mol, in the case of **IMCb** it is exergonic by −5.5 kcal/mol.

From **INa**, the activation free energy to obtain the formal [4 + 2] cycloadduct $\mathbf{4a}^{\bullet+}$ via **TS3a** is 11.2 kcal/mol, a barrier easy to overcome under the usual reaction conditions. A similar behavior is found for **INb** along the reaction pathway ii, where the activation free energy for the formation of $\mathbf{4b}^{\bullet+}$ via **TS3b** is 10.5 kcal/mol.

Geometries of the Stationary Points. The gas-phase geometries of the transition states and intermediates involved in the reactions of $\mathbf{1a,b}^{\bullet+}$ are shown in Figure 2.

At **TS1a** and **TS1b**, the lengths of the C2−C3 bonds are 1.894 and 1.893 Å, while the lengths of the S−C4 bonds are 1.855 and 1.872 Å, respectively. At **TS1a′** the length of the C2−C3 bond is 1.527 Å, while the length of the S−C4 breaking bond is 2.804 Å (see geometry of **TS1a′** in Figure S1 of the Supporting Information). At intermediates **INa** and **INb**, the corresponding values for the S−C4 bonds are 1.958 and 2.070 Å, while the distance between C2 and C3 is 3.681 and 3.759 Å, respectively. Accordingly, while the C4 carbon remains pyramidalized at **INa, b**, the C2 and C3 carbons are planar as expected for a sp^2 hybridization. At **TS2a** and **TS2b**, the lengths of the S−C4 bonds are 2.289 and 2.097 Å, respectively. It is noteworthy that although **INb** and **TS2b** are quite close both in energy and geometry, they are clearly characterized by frequency analysis. Thus, while **INb** has no imaginary frequency, **TS2b** has a unique imaginary frequency, −37.1 cm^{-1}, associated mainly with S−C4 bond breaking. Finally, at **TS3a** and **TS3b**, the lengths of the C3−C6 forming bonds are 2.157 and 2.172 Å, while the lengths of the S−C4 bonds are 1.911 and 1.900 Å, respectively.

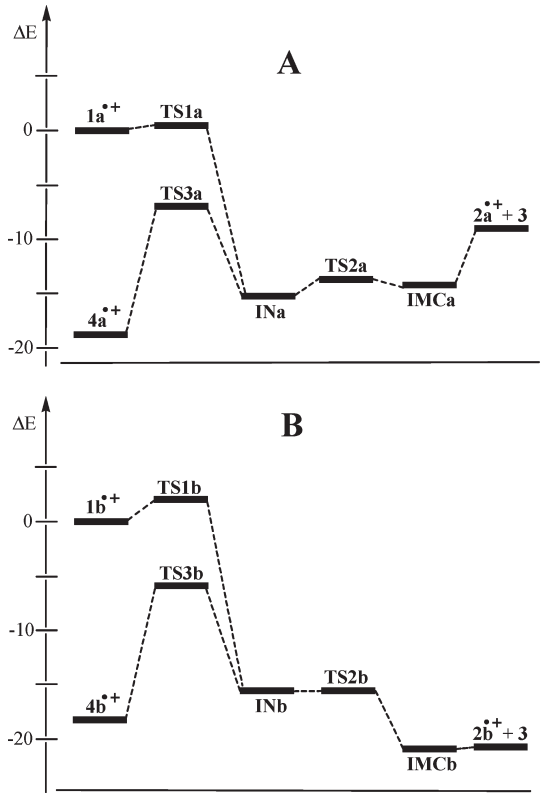

Figure 1. Energy profiles, in kcal/mol, for the stepwise CR of $\mathbf{1a}^{\bullet+}$ (A) and $\mathbf{1b}^{\bullet+}$ (B) in acetonitrile.

Table 2. UB3LYP/6-31G* Total and Relative Enthalpies (H, in au, and ΔH, in kcal/mol), Entropies (S, and ΔS, in cal/(mol K)), and Free Energies (G, in au, and ΔG, in kcal/mol) Computed at 298.15 K and 1 atm in Acetonitrile of the Transition States, Intermediates, and Ion−Molecule Complexes Involved in the CR of $\mathbf{1a,b}^{\bullet+}$

	H	ΔH	S	ΔS	G	ΔG
$\mathbf{1a}^{\bullet+}$	−1247.994454		150.2		−1248.065809	
TS1a	−1247.993045	0.9	152.2	2.1	−1248.065374	0.3
INa	−1248.020179	−16.1	157.4	7.2	−1248.094946	−18.3
TS2a	−1248.017575	−14.5	148.0	−2.1	−1248.087916	−13.9
IMCa	−1248.018025	−14.8	148.3	−1.9	−1248.088490	−14.2
$\mathbf{2a}^{\bullet+}$ + **3**	−1248.009891	−9.7	204.8	54.6	−1248.107193	−26.0
TS3a	−1248.005379	−6.9	151.1	0.9	−1248.077178	−7.1
$\mathbf{4a}^{\bullet+}$	−1248.022519	−17.6	145.8	−4.4	−1248.091795	−16.3
$\mathbf{1b}^{\bullet+}$	−1439.681916		157.1		−1439.756540	
TS1b	−1439.677925	2.5	159.7	2.6	−1439.753787	1.7
INb	−1439.706370	−15.3	164.2	7.2	−1439.784401	−17.5
TS2b	−1439.705960	−15.1	165.4	8.3	−1439.784526	−17.6
IMCb	−1439.715650	−21.2	163.2	6.1	−1439.793178	−23.0
$\mathbf{2b}^{\bullet+}$ + **3**	−1439.715126	−20.8	217.3	60.2	−1439.818391	−38.8
TS3b	−1439.689782	−4.9	164.0	6.9	−1439.767687	−7.0
$\mathbf{4b}^{\bullet+}$	−1439.707543	−16.1	159.0	1.9	−1439.783109	−16.7

dx.doi.org/10.1021/jp200177a |*J. Phys. Chem. A* 2011, 115, 5443–5448

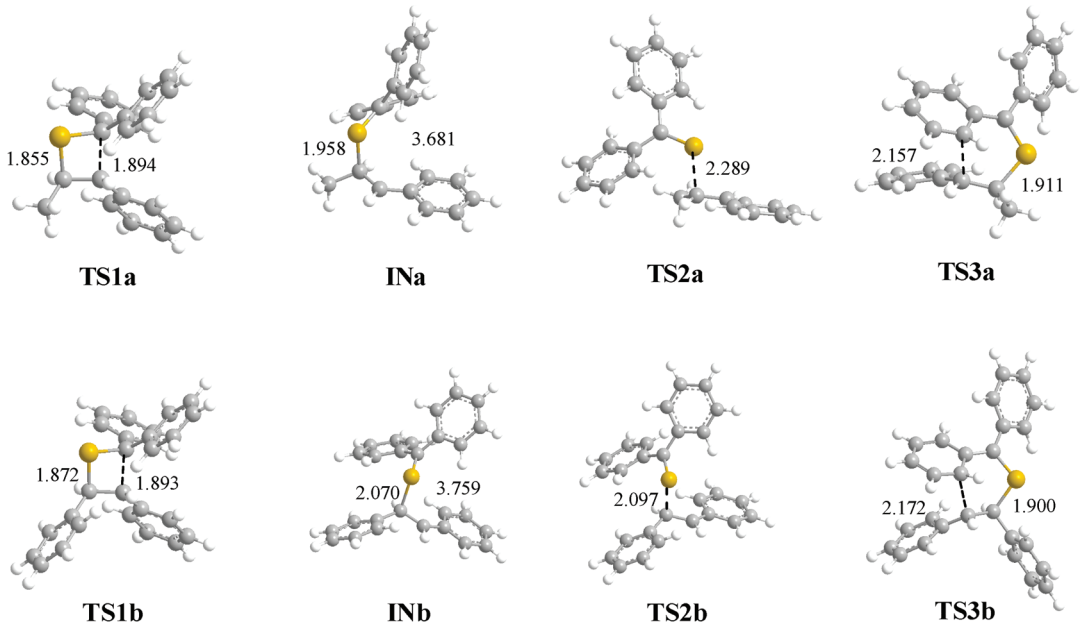

Figure 2. Structures of transition states and intermediates involved in the stepwise CR of radical cations $\mathbf{1a}^{\bullet+}$ and $\mathbf{1b}^{\bullet+}$.

Table 3. UB3LYP/6-31G* Total Atomic Spin Densities for the Stationary Points along the CR of Radical Cations $\mathbf{1a,b}^{\bullet+}$

	$\mathbf{1a}^{\bullet+}$	INa	IMCa	$\mathbf{2a}^{\bullet+}$	$\mathbf{4a}^{\bullet+}$
S1	0.42	0.02	0.42	–	0.12
C2	−0.03	0.19	−0.03	–	0.16
C3	0.01	0.50	0.21	0.41	0.04
C4	−0.01	−0.03	0.14	0.06	0.00
	$\mathbf{1b}^{\bullet+}$	INb	IMCb	$\mathbf{2b}^{\bullet+}$	$\mathbf{4b}^{\bullet+}$
S1	0.40	0.06	0.30	–	0.12
C2	−0.02	0.16	−0.02	–	0.15
C3	0.03	0.48	0.21	0.17	0.00
C4	0.00	−0.02	0.12	0.17	0.04

At the IMCs, the distance between the sulfur atom and C4 is 2.823 (**IMCa**) and 3.117 Å (**IMCb**); the geometries of IMCs are shown in the Supporting Information, Figure S2. The shorter distance at the more energetic **IMCa** suggests a tighter electronic interaction between both fragments.

Bond Order Analysis of the Stationary Points. The electronic structure of the TSs and intermediates of these reactions was analyzed by using the bond orders BOs.[20] At **TS1a** and **TS1b**, the BO values of the C2−C3 bonds are 0.61 and 0.61, while those of the corresponding S−C4 bonds are 0.98 and 0.94. At intermediates **INa** and **INb**, the BO values of the S−C4 bonds are 0.83 and 0.72, respectively. The C3−C(ipso) BO values at **INa,b**, ca. 1.30, are in agreement with some π character of the bond, as a consequence of benzylic conjugation, which accounts for the remarkable stabilization of these intermediates. At **TS2a** and **TS2b**, the BO values of the S−C4 bonds are 0.55 and 0.74. Finally, at **TS3a,b**, the BO values of the C3−C6 and S−C4 bonds are 0.37 and 0.91, respectively.

Spin and Charge Analysis. A comparative analysis of the atomic spin densities for the stationary points indicates that the thietane framework undergoes a similar spin redistribution for $\mathbf{1a}^{\bullet+}$ and $\mathbf{1b}^{\bullet+}$ along the two mechanistic pathways (see Table 3 and Figure S3 in the Supporting Information). The main difference was found between the IMCs, where the sulfur atom has a larger spin density at the more energetic **IMCa**.

Thus, radical cations $\mathbf{1a,b}^{\bullet+}$ have a large spin concentration at the S atom, 0.4. By contrast, at intermediates **INa,b** most of the spin density is located on C3, 0.5, although the two ortho positions of the phenyl substituent at C3 also support some spin density (0.16 each one). These changes point to a homolytic C2−C3 bond breaking, which is also supported by the similar Mulliken atomic charges found at the C3 atom of $\mathbf{1a}^{\bullet+}$ (−0.21 e) and **INa** (−0.16 e).

After S−C4 bond cleavage at intermediates **INa,b**, a large spin density is accumulated at the sulfur atom of the IMCs: 0.42 (**IMCa**) and 0.30 (**IMCb**). This can be understood by a strong interaction between the S atom of neutral **3** and the C4 carbon of radical cations $\mathbf{2a}^{\bullet+}$ and $\mathbf{2b}^{\bullet+}$; actually, the S−C4 distance at **IMCa** and **IMCb** is only 2.824 and 3.117 Å, respectively. The shorter value found at **IMCa** accounts for a larger interaction between the two fragments at this IMC and for the higher spin density located at the sulfur atom of this complex. In **IMCb**, the ortho and para positions of the aryl substituent at C4 have also some spin density (a total of 0.33) indicating a significant participation of this substituent. The electronic nature of the IMCs was studied by analysis of their atomic natural charges, which were found to be shared between the TBP and the alkene fragments. The obtained values were 0.49 e at **3** and 0.51 e at **2a** for **IMCa**, as compared with 0.34 at **3** and 0.66 e at **2b** for **IMCb**. This indicates a large degree of charge transfer between the neutral and radical cationic units, which is less marked for the more delocalized **IMCb**.

The radical cation of *trans*-β-methylstyrene $\mathbf{2a}^{\bullet+}$ has a larger spin concentration at the C3 position (0.41) than at C4 (0.06), whereas *trans*-stilbene radical cation $\mathbf{2b}^{\bullet+}$ presents a symmetric spin distribution at the C3 and C4 positions (0.17). Finally, cycloadducts $\mathbf{4a,b}^{\bullet+}$ present a similar spin density distribution at the four atoms of the starting thietane ring. In these species the spin density is mainly located at ortho and para position of the phenyl substituents of the thiocarbonyl group.

dx.doi.org/10.1021/jp200177a |*J. Phys. Chem. A* 2011, 115, 5443–5448

CONCLUSIONS

The reaction pathways associated with formation of the CR products **2a,b** plus **3**, or the formal [4 + 2] cycloadduct **5**, in the PET reactions of thietanes **1a,b** have been studied theoretically using DFT methods at the UB3LYP/6-31G* level. These reactions follow stepwise mechanisms, which are initiated by C2−C3 bond breaking to give radical cationic intermediates **INa,b**. Then, two competitive reaction pathways are feasible. In pathway i, S−C4 bond breaking affords the alkene radical cations $\mathbf{2a}^{\bullet+}$ and $\mathbf{2b}^{\bullet+}$ plus neutral TBP **3**, via tightly bound ion−molecule complexes (IMCs). In pathway ii, intramolecular attack of the C3 carbon of **INa,b** to the ortho position of the phenyl substituent at C2 yields the radical cationic [4 + 2] cycloadducts $\mathbf{4a,b}^{\bullet+}$.

This picture is basically coincident with the previously proposed mechanism, based only on experimental results. Thus, it is confirmed that IMCs play a key role in the competition between CR and rearrangement to formal [4 + 2] cycloaddition products. Interestingly, the systematic theoretical study performed in the present work has allowed us to characterize the INs as additional stationary points, providing a more complete description of the mechanism. In addition, the experimental results suggested that competition between escape of free radical ions from the IMCs and formal [4 + 2] cycloaddition depends on the relative energy barriers. This is also confirmed by the present calculation, which clearly shows that the relative energy of **TS3b** (compared to $\mathbf{2b}^{\bullet+}$ + **3**) is much higher than in the case of **TS3a**/$\mathbf{2a}^{\bullet+}$ + **3**.

The electronic structures of the species involved in these reactions suggest that the higher stability of the radical cationic of *trans*-stilbene ($\mathbf{2b}^{\bullet+}$) compared to that of *trans*-2-methylstyrene ($\mathbf{2a}^{\bullet+}$) is responsible for differentiated reactivity of the two thietanes. This can be attributed to the substituent effects, as the additional phenyl group of $\mathbf{2b}^{\bullet+}$ facilitates effective delocalization of charge and spin in this radical ion and favors its escape from **IMCb**, as compared to the **IMCa**/$\mathbf{2a}^{\bullet+}$ system.

ASSOCIATED CONTENT

Supporting Information. Figures with structures of **TS1a′**, **IMCa**, and **IMCb**. Table containing MPWB1K/6-31G* thermodynamic data of CR products $\mathbf{2a,b}^{\bullet+}$ + **3**, **IMCa,b**, and rearranged products $\mathbf{4a,b}^{\bullet+}$. Figures with the spin density of radical cations and intermediates involved in the CR of thietane radical cations $\mathbf{1a,b}^{\bullet+}$. Total energies computed by (U)B3LYP/6-31G*, unique imaginary frequency, and Cartesian coordinates of the stationary points involved in the CR of thietane radical cations $\mathbf{1a,b}^{\bullet+}$. This material is available free of charge via the Internet at http://pubs.acs.org.

AUTHOR INFORMATION

Corresponding Author

*E-mail: domingo@utopia.uv.es (L.R.D.); mmiranda@qim.upv.es (M.A.M).

ACKNOWLEDGMENT

The Spanish Government (Grants No. CTQ2009-11027 and CTQ2009-13699), the UPV (Grant No. 20100994), and Fundación CajaMurcia (postdoctoral fellowship to R.P.-R.) are gratefully acknowledged.

REFERENCES

(1) (a) Accorsi, G.; Armaroli, N. *J. Phys Chem. C* **2010**, *114*, 1385–1403. (b) Doose, S.; Neuweiler, H.; Sauer, M. *ChemPhysChem* **2009**, *10*, 1389–1398. (c) Hoffmann, N. *Chem. Rev.* **2008**, *108*, 1052–1103. (d) Hoffmann, N. *J. Photochem. Photobiol., C* **2008**, *9*, 43–60. (e) Griesbeck, A. G.; Hoffmann, N.; Warzecha, K.-D. *Acc. Chem. Res.* **2007**, *40*, 128–140. (f) Schmoldt, P.; Rinderhagen, H.; Mattay, J. *Mol. Supramol. Photochem.* **2003**, *9*, 185–225. (g) Oelgemöller, M.; Giresbeck, A. G. *J. Photochem. Photobiol., C* **2002**, *3*, 109–127. (h) Lewis, F. D.; Wu, Y. *J. Photochem. Photobiol., C* **2001**, *2*, 1–16. (i) Schmittel, M.; Burghart, A. *Angew. Chem., Int. Ed. Engl.* **1997**, *36*, 2550–2589. (j) Müller, F.; Mattay, J. *Chem. Rev.* **1993**, *93*, 99–117.

(2) (a) Sadeghian, K.; Bocola, M.; Merz, T.; Schütz, M. *J. Am. Chem. Soc.* **2010**, *132*, 16285–16295. (b) Boussicault, F.; Robert, M. *Chem. Rev.* **2008**, *108*, 2622–2645. (c) Beukers, R.; Eker, A. P. M.; Lohman, P. H. M. *DNA Repair* **2008**, *7*, 530–543. (d) Borg, O. A.; Eriksson, L. A.; Durbeej, B. *J. Phys. Chem. A* **2007**, *111*, 2351–2361. (e) Stafforst, T.; Diederichsen, U. *Chem. Commun.* **2005**, 3430–3432. (f) Sancar, A. *Chem. Rev.* **2003**, *103*, 2203–2237. (g) Cichon, M. K.; Arnold, S.; Carell, T. *Angew. Chem., Int. Ed.* **2002**, *41*, 767–770. (h) Joseph, A.; Prakash, G.; Falvey, D. E. *J. Am. Chem. Soc.* **2000**, *122*, 11219–11225. (i) Wang, Y.; Gaspar, P. P.; Taylor, J. S. *J. Am. Chem. Soc.* **2000**, *122*, 5510–5519. (j) Kim, S.-T.; Malhorta, K.; Smith, C. A.; Taylor, J. S.; Sancar, A. *J. Biol. Chem.* **1994**, *269*, 8535–8540.

(3) (a) Andreu, I.; Delgado, J.; Espinós, A.; Pérez-Ruiz, R.; Jiménez, M. C.; Miranda, M. A. *Org. Lett.* **2008**, *10*, 5207–5210. (b) Trzcionka, J.; Lhiaubet-Vallet, V.; Paris, C.; Belmadoui, N.; Climent, M. J.; Miranda, M. A. *ChemBioChem* **2007**, *8*, 402–407. (c) Pérez-Ruiz, R.; Miranda, M. A.; Alle, R.; Meerholz, K.; Griesbeck, A. G. *Photochem. Photobiol. Sci.* **2006**, *5*, 51–55. (d) Pérez-Ruiz, R.; Gil, S.; Miranda, M. A. *J. Org. Chem.* **2005**, *70*, 1376–1381. (e) Izquierdo, M. A.; Miranda, M. A. *Eur. J. Org. Chem.* **2004**, 1424–1431. (f) Pérez-Ruiz, R.; Izquierdo, M. A.; Miranda, M. A. *J. Org. Chem.* **2003**, *68*, 10103–10108. (g) Miranda, M. A.; Izquierdo, M. A.; Pérez-Ruiz, R. *J. Phys. Chem. A* **2003**, *107*, 2478–2482. (h) Miranda, M. A.; Izquierdo, M. A. *Chem. Commun.* **2003**, 364–365. (i) Miranda, M. A.; Izquierdo, M. A. *J. Am. Chem. Soc.* **2002**, *124*, 6532–6533. (j) Miranda, M. A.; Izquierdo, M. A.; Galindo, F. *J. Org. Chem.* **2002**, *67*, 4138–4142. (k) Miranda, M. A.; Izquierdo, M. A.; Galindo, F. *Org. Lett.* **2001**, *3*, 1965–1968.

(4) Izquierdo, M. A.; Domingo, L. R.; Miranda, M. A. *J. Phys.Chem. A* **2005**, *109*, 2602–2607.

(5) Friedel, M. G.; Cichon, M. K.; Carell, T. *Org. Biomol. Chem.* **2005**, *3*, 1937–1941.

(6) Shima, K.; Sazaki, A.; Nakabayashi, K.; Yasuda, M. *Bull. Chem. Soc. Jpn.* **1992**, *65*, 1472–1474.

(7) Argüello, J. E.; Pérez-Ruiz, R; Miranda, M. A. *Org. Lett.* **2010**, *12*, 1884–1887.

(8) (a) Becke, A. D. *J. Chem. Phys.* **1993**, *98*, 5648–5652. (b) Lee, C.; Yang, W.; Parr, R. G. *Phys. Rev. B* **1988**, *37*, 785–789.

(9) Hehre, W. J.; Radom, L.; Schleyer, P. v. R.; Pople, J. A. *Ab Initio Molecular Orbital Theory*; Wiley: New York, 1986.

(10) Domingo, L. R.; Pérez-Prieto, J. *ChemPhysChem* **2006**, *7*, 614–618.

(11) (a) Schlegel, H. B. *J. Comput. Chem.* **1982**, *3*, 214. (b) Schlegel, H. B. Geometry optimization on potential energy surface. In *Modern Electronic Structure Theory*; World Scientific: Singapore, 1994.

(12) Fukui, K. *J. Phys. Chem.* **1970**, *74*, 4161–4163.

(13) (a) González, C.; Schlegel, H. B. *J. Phys. Chem.* **1990**, *94*, 5523–5527. (b) González, C.; Schlegel, H. B. *J. Chem. Phys.* **1991**, *95*, 5853–5860.

(14) Reed, A. E.; Weinstock, R. B.; Weinhold, F. *J. Chem. Phys.* **1985**, *83*, 735–746.

(15) (a) Tomasi, J.; Persico, M. *Chem. Rev.* **1994**, *94*, 2027–2094. (b) Simkin, B. Y.; Sheikhet, I. *Quantum Chemical and Statistical Theory of Solutions—A Computational Approach*; Ellis Horwood: London, 1995.

(16) (a) Cances, E.; Mennucci, B.; Tomasi, J. *J. Chem. Phys.* **1997**, *107*, 3032–3041. (b) Cossi, M.; Barone, V.; Cammi, R.; Tomasi, J. *Chem. Phys. Lett.* **1996**, *255*, 327–335. (c) Barone, V.; Cossi, M.; Tomasi, J. *J. Comput. Chem.* **1998**, *19*, 404–417.

(17) Scott, A. P.; Radom, L. *J. Phys. Chem.* **1996**, *100*, 16502–16513.
(18) Frisch, M. J.; Trucks, G. W.; Schlegel, H. B.; Scuseria, G. E.; Robb, M. A.; Cheeseman, J. R.; Zakrzewski, V. G.; Montgomery, J. A., Jr.; Stratmann, R. E.; Burant, J. C.; Dapprich, S.; Millam, J. M.; Daniels, A. D.; Kudin, K. N.; Strain, M. C.; Farkas, O.; Tomasi, J.; Barone, V.; Cossi, M.; Cammi, R.; Mennucci, B.; Pomelli, C.; Adamo, C.; Clifford, S.; Ochterski, J.; Petersson, G. A.; Ayala, P. Y.; Cui, Q.; Morokuma, K.; Malick, D. K.; Rabuck, A. D.; Raghavachari, K.; Foresman, J. B.; Cioslowski, J.; Ortiz, J. V.; Stefanov, B. B.; Liu, G.; Liashenko, A.; Piskorz, P.; Komaromi, I.; Gomperts, R.; Martin, R. L.; Fox, D. J.; Keith, T.; Al-Laham, M. A.; Peng, C. Y.; Nanayakkara, A.; González, C.; Challacombe, M.; Gill, P. M. W.; Johnson, B. G.; Chen, W.; Wong, M. W.; Andres, J. L.; Head-Gordon, M.; Replogle, E. S.; Pople, J. A. *Gaussian 98*, revision A.6; Gaussian, Inc.: Pittsburgh, PA, 1998.
(19) Lynch, B. J.; Fast, P. L.; Harris, M.; Truhlar, D. G. *J. Phys. Chem. A* **2000**, *104*, 4811–4815.
(20) Wiberg, K. B. *Tetrahedron* **1968**, *24*, 1083–1096.